RESEARCH ARTICLE | APRIL 24 2023

Evaluation protocol for revealing magnonic contrast in TR-STXM measurements

Benjamin Zingsem; Thomas Feggeler ✉; Ralf Meckenstock; ... et. al

AIP Advances 13, 045020 (2023)
https://doi.org/10.1063/5.0145753

Evaluation protocol for revealing magnonic contrast in TR-STXM measurements

Cite as: AIP Advances 13, 045020 (2023); doi: 10.1063/5.0145753
Submitted: 7 February 2023 • Accepted: 31 March 2023 •
Published Online: 24 April 2023

Benjamin Zingsem,[1,2] Thomas Feggeler,[1,3,6,a)] Ralf Meckenstock,[1] Detlef Spoddig,[1] Taddäus Schaffers,[4] Santa Pile,[4] Hendrik Ohldag,[3,5,7,8] Michael Farle,[1] Heiko Wende,[1] Andreas Ney,[4] and Katharina Ollefs[1]

AFFILIATIONS

[1] Faculty of Physics and Center for Nanointegration (CENIDE), University of Duisburg-Essen, 47057 Duisburg, Germany
[2] Ernst Ruska Centre for Microscopy and Spectroscopy with Electrons and Peter Grünberg Institute, Forschungszentrum Jülich GmbH, 52425 Jülich, Germany
[3] Advanced Light Source, Lawrence Berkeley National Laboratory, Berkeley, California 94720, USA
[4] Institut für Halbleiter- und Festkörperphysik, Johannes Kepler University, 4040 Linz, Austria
[5] SLAC National Accelerator Laboratory, Menlo Park, California 94025, USA
[6] Department of Physics, University of California Berkeley, Berkeley, California 94720, USA
[7] Department of Material Sciences and Engineering, Stanford University, Stanford, California 94305, USA
[8] Department of Physics, University of California Santa Cruz, Santa Cruz, California 95064, USA

[a)] **Author to whom correspondence should be addressed:** tfeggeler@lbl.gov

ABSTRACT

We present a statistically motivated method to extract magnonic contrast from time-resolved scanning transmission x-ray microscopy (TR-STXM) measurements. TR-STXM is an element-specific method for resolving spin-dynamics in space and time. It offers nanometer spatial resolution and picosecond temporal resolution. The presented method makes it possible to obtain phase and amplitude profiles of spin-waves from STXM measurements. Furthermore, it allows for a rigorous transformation to reciprocal magnon $\vec{k}$-space, revealing $\vec{k}$-dependent magnon properties such as the magnon dispersion in three dimensions and for all directions of the magnetic anisotropy. We demonstrate our method using X-band ferromagnetic resonance on a micrometer-sized permalloy assembly.

INTRODUCTION

Collective oscillatory spin states, called magnons, can be excited in magnetic materials at microwave frequencies. Their spectral characteristics are determined by and serve as a characterization method for all magnetic parameters in a magnetic system.[1] Magnons can be used as carriers of information in data processing, such as quantum computing and spin-wave logic,[2–6] with the potential to supersede conventional electronics in many ways.[6] For example, energy efficiency, requirements for heat dissipation, and logic gate density (in analogy to transistor density).[5] Various established techniques are employed for measuring magnonic excitations. The most prominent ones include Ferromagnetic Resonance (FMR),[7] Brillouin light scattering (BLS),[8] neutron scattering,[9,10] Scanning Electron Microscopy (SEM) with polarization analyzer (SEMPA),[11] and spin-polarized scanning tunneling microscopy (SP-STM),[12] to name a few. FMR spectroscopy is used to investigate spectral properties, while BLS is a surface-sensitive technique to measure the spatial distribution of spin-waves down to the resolution limit of visible light.[8]

The spatially resolved extraction of amplitude and phase of magnons discussed in this work applies to a combination of Scanning Transmission X-Ray Microscopy (STXM) with FMR.[13–18] Here, the effect of X-ray Magnetic Circular Dichroism (XMCD) is used, where the scattering of circular polarized x-rays with electrons in a material depends on the spin of the electrons involved, i.e., the occupation of minority and majority spin channels in the electron density of states.[19] In the following, we discuss an evaluation

technique to extract magnonic information from such measurements beyond the application of time-FFT[20] algorithms and time domain fits.[17,18] This includes the spectral and spatial resolution of magnonic eigenstates in real and reciprocal space, as well as the extraction of the spin-wave dispersion with quantitative statistical significance.

MAIN BODY

Experimental setup and measurement technique

The experimental setup combining a Ferromagnetic Resonance spectrometer and a Scanning Transmission X-Ray Microscope allows for element-specific and time-resolved characterization of magnetization dynamics with high spatial resolution[13] down to 10 nm.[21] Using x-ray magnetic circular dichroism (XMCD), a contrast proportional to the difference in the number of minority and majority spins at the 3D orbitals is detected. For this purpose, circular polarized x-rays are focused on the sample using a zone plate. The transmitted x-rays are detected by an x-ray avalanche photodiode located behind the sample.[13] A static magnetic field is applied perpendicular to the wavevector of the x rays with a slight rotation of 3° off of the horizontal axis of the sample (Fig. 1). The field was varied from 82 to 110 mT in steps of 2 mT. The sample itself is positioned in a microresonator[22] such that a microwave magnetic field is applied perpendicular to the static field and parallel to the x-ray propagation direction. The microwave frequency is synchronized to the klystron frequency of the synchrotron [Stanford Synchrotron Radiation Lightsource (SSRL): 476.315 MHz]. The synchronization scheme employs a phase-locked loop comparing the output of the microwave source with the nth harmonic of the klystron frequency and adjusting the generator's output frequency correspondingly. In this case, a microwave frequency of 9.446 GHz is selected, which corresponds to the 20th harmonic of the klystron frequency subtracted by 1/6 of the klystron frequency (see Ref. 13 for details). Using this setup, we are detecting *only 6 points in time of a microwave cycle* with a time distance of 18 ps; each of the points is measured with the microwave on/off, respectively, with the same electron bunch. As the frequency of the electron bunches (bunch length of 50 ps) in the storage ring of the synchrotron is 1.28 MHz, a rectangular modulation of the microwaves is implemented at this frequency using a PIN diode, attenuating the microwaves by −35 dB. The data received from the x-ray diode are stored in a device providing 12 *slots*, the first 6 of which record the signal with microwaves turned on, whereas the x-ray signal with microwaves turned off is stored in the remaining 6 slots.[13]

The data used in this work to demonstrate our evaluation protocol have been obtained for a sample that consists of two Py stripes in a T-shape arrangement, spaced 2 μm apart (Fig. 1). Each stripe has lateral dimensions of 5 μm by 1 μm and a thickness of 30 nm. The same data have been used in Ref. 14, where a real space visual comparison was used to interpret the data.

Evaluation method

To extract time-dependent oscillations in the MW-On state, the count rate in the MW-Off state has to be compared to that in the MW-On state at each position as a means of normalization. It becomes apparent that the results will be similar regardless of whether the ratio or the difference of ON/OFF states is used to compare those when considering

$$\frac{a_{x,y}(t)}{b_{x,y}(t)} = \frac{a_{x,y}(t) - b_{x,y}(t)}{b_{x,y}(t)} + 1, \tag{1}$$

where $a_{x,y}(t)$ is the count rate at pixel x, y, and time t in the MW-On state, and similarly, $b_{x,y}(t)$ is the count rate in the MW-Off state. It can be motivated by the count rate without MW $b_{x,y}(t) = b_{x,y}$ is roughly constant in time, as no spin waves are excited. From there, with Eq. (1), the proportionality

$$\frac{a_{x,y}(t)}{b_{x,y}(t)} \propto a_{x,y}(t) - b_{x,y}(t), \tag{2}$$

follows. The influence of noise (or a signal other than the desired magnonic contrast), however, is vastly different when comparing ratio and difference as a means of relating the signals. This can be estimated through the gradient of the left and right sides of Eq. (2) in quantities a and b, where

$$\nabla_{a,b}\left(\frac{a}{b}\right) = \begin{pmatrix} \frac{1}{b} \\ -\frac{a}{b^2} \end{pmatrix}, \tag{3}$$

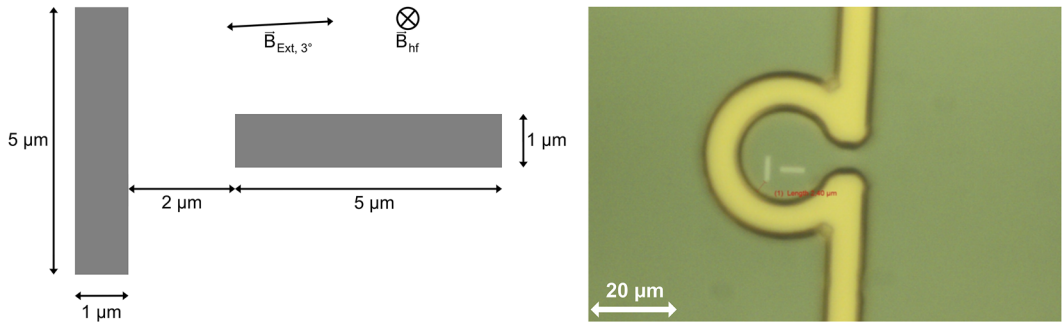

FIG. 1. Schematic representation of the sample (left) and optical microscopy image of the sample as placed in the μ-resonator (right). Two permalloy stripes with dimensions of 5 μm by 1 μm in perpendicular orientation. The stripes have a thickness of 30 nm and are separated by a gap of 2 μm. Details of the sample preparation, along with an in-depth discussion of the STXM characterization, can be found in Ref. 14. During the measurement, a static magnetic field B_{Ext} is applied with a slight rotation of 3° off of the horizontal axis. Additionally, an FMR like excitation is driven by a microwave field B_{hf} perpendicular to the sample plane. A microwave frequency of 9.446 GHz is used.

$$\nabla_{a,b}(a-b) = \begin{pmatrix} -b \\ a \end{pmatrix}. \tag{4}$$

Hence, fluctuations in b have a non-linear effect on fluctuations in the ratio, whereas fluctuations in a and b have a linear effect on fluctuations in the difference. Therefore, the signal-to-noise ratio should be considered when deciding how to compare MW-On and MW-Off signals. Except for the perceived noise level, these operations yield equivalent results in the evaluation of magnonic contrast, and both can be used in quantitative analysis as one can be transformed into the other using Eq. (1).

A sine-like magnonic response to the sine-like microwave excitation is expected, such that the magnonic contrast can now be extracted by fitting a sine-function to the time-dependent data at each point on the sample that was normalized using one of the methods above. In addition, it is expected that the dynamic response of the sample oscillates at the same frequency as the microwave driving it. Figure 2(b) depicts a sine wave fitted into the time-dependent signal at one point on the sample. The model is given as

$$A \sin\left(2\pi \frac{\omega}{\omega_0} t + \phi\right) + d, \tag{5}$$

where A accounts for the amplitude of the oscillation, ω_0 is the excitation frequency, t is the time in periods, ϕ accounts for a phase shift relative to $t = 0$, and d describes an offset, which is usually close to 0 for the case of $a - b$ and close to 1 when analyzing $\frac{a}{b}$. Note that only A, ϕ and d are free parameters in the fit, and the physical assumption is that $\omega = \omega_0$.

Having performed this fit at each pixel, we can now extract the spatial distribution of the fit parameters, i.e., the spatial distribution of amplitude and phase. The resulting spatial map of, e.g., the amplitude and phase profile now serves as a noise free representation of the magnon distribution in the sample. Additionally, a simple measure for the validity of this fit can be given by the statistical p-value. It measures the likelihood that the dataset to which the fit was applied originates from a random distribution rather than a distribution following the assumed model. The p-value, therefore, gives a measure for how adequate our fit is at each pixel, where small p-values indicate a good fit. These three values can then be encoded in an image, as seen in Fig. 2(a)(v). Here, the *hue, saturation, brightness* (HSB) color scale was used, where the phase was encoded into the *hue* channel, the amplitude was encoded into the *brightness* channel, and one minus the p-value $(1 - p)$ was encoded into the saturation. Therefore, bright pixels correspond to high amplitudes, while highly saturated pixels correspond to a very sine-like oscillation. One can quickly spot that encoding this information

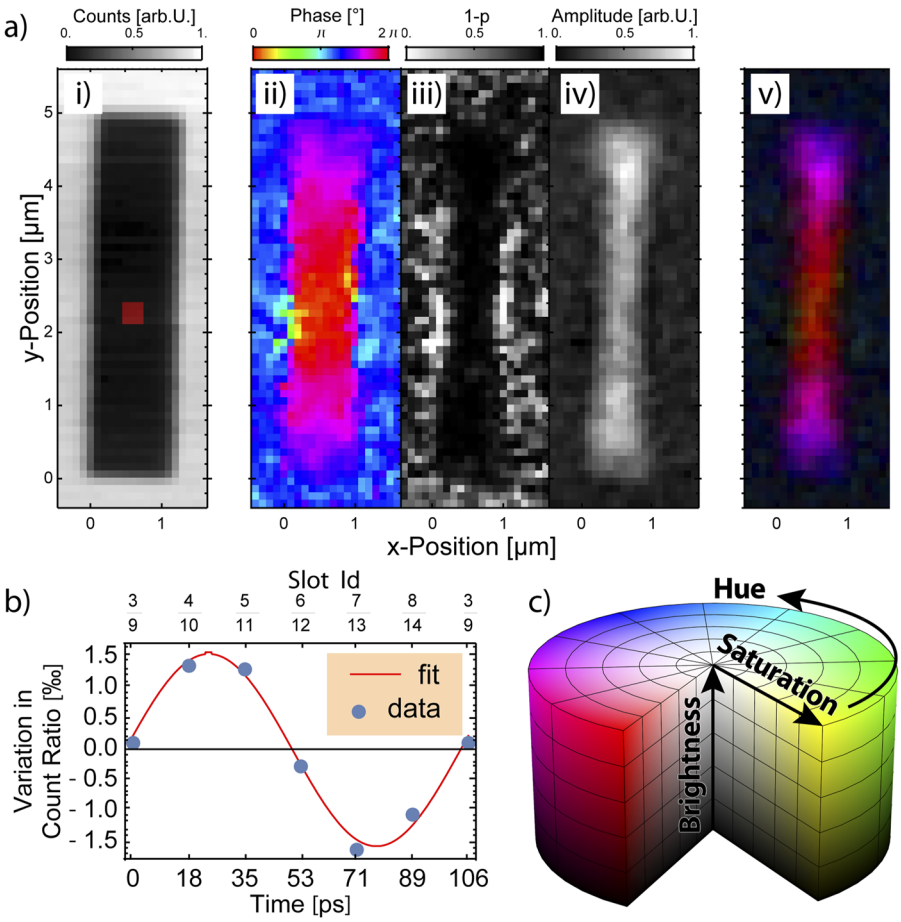

FIG. 2. Magnonic contrast image. (a)(i) Depiction of the x-ray transmission count rate across the sample. (ii)–(iv) color channels used to encode magnonic information, where (ii) depicts the phase distribution encoded as the cyclic hue channel, (iii) represents the p-value of the statistical analysis at each pixel, encoded as the saturation, and (iv) represents the spin-wave amplitude encoded as the brightness value in (v). (v) Assembled HSB image of the magnonic excitation. b) time-dependent recording acquired in the red region in the center of (a)(i). (c) Three-dimensional representation of the HSB color scale as used in (a)(v).

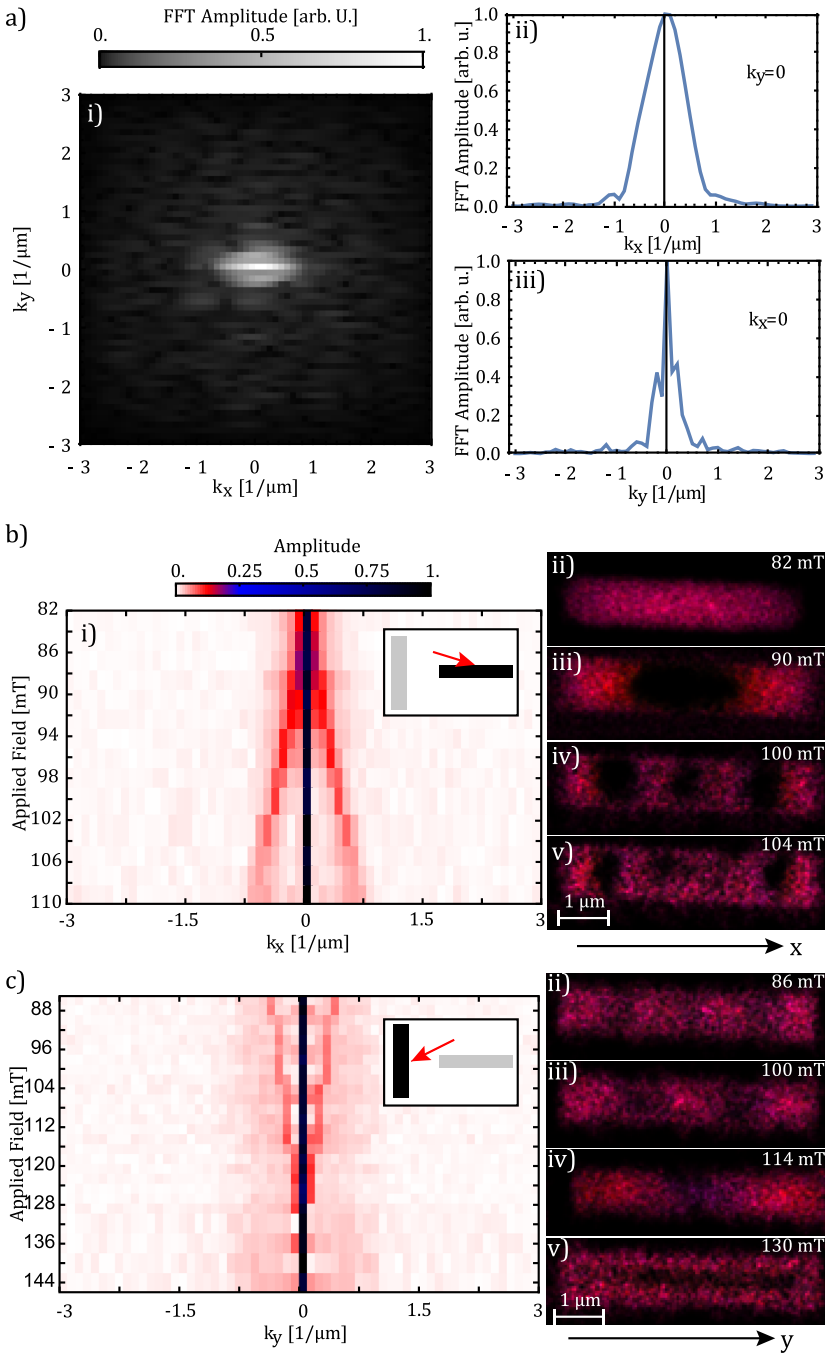

FIG. 3. Spatial Fourier transformation of the phase and amplitude values depicted in Figs. 2(a)(ii) and 2(a)(iv). (a) FFT in two spatial dimensions (i) and along the cardinal directions (ii) and (iii). The k_x dependence shows a broad distribution around $k_x = 0$, which is most likely dominated by the spatial confinement of the sample itself. The k_y distribution, on the other hand, shows a narrow distribution around $k_y = 0$ with two distinct modes visible at $k_y = \pm 0.2\ \mu\text{m}^{-1}$, which demonstrates that the observed oscillation is composed of two counter-propagating waves with a wavelength of about 5 μm. (b) Reconstruction of the spin-wave dispersion in the horizontal stripe [see inset (b)(i)]. The reconstruction is obtained from field-dependent STXM measurements at a fixed frequency of 9.446 GHz. The field was swept from 82 to 110 mT in steps of 2 mT. The colored dispersion in (i) shows the spin-wave amplitude [similar to (a)(iii)] for all k-vectors and all applied field values at $k_y = 0$. (ii)–(v) exemplarily depict some of the mode profiles used in FFT evaluation (compare Fig. 2 for color legends). The black stripe at $k_x = 0$ indicates a strong $k = 0$ contribution at all field values due to the excitation setup. (c) Shows the same evaluation as (b), plotted for the vertical stripe (see inset).

into an image like this immediately reveals the spatial structure of the excited magnonic eigenstate, including phase information. The next task is to investigate the $\vec{k}$-vectors this state comprises. This can be achieved by introducing a complex value $z_{x,y}$ at each pixel x, y, where $\|z_{x,y}\| = A$ and $\arg(z_{x,y}) = \phi$. Applying a Fourier transformation to the spatial coordinates x and y transforms the spatial wave to reciprocal space, revealing the $\vec{k}$-vectors involved in this state [Fig. 3(a)]. A similar attempt was made in Ref. 16; it was, however, not conclusive. Our method of isolating the relevant wave parameters first, in contrast, yields conclusive results even if the data density is minimal in the time domain (compare Figs. 2 and 3). When performing measurements at a fixed frequency and different fields, or different frequencies and a fixed field, this can be used to reveal the spin-wave dispersion [Figs. 3(b) and 3(c)]. Figure 3 illustrates the $\vec{k}$ resolution for the spatial eigenstate observed in Fig. 2. The broad distribution around $\vec{k}_x = 0$ [Fig. 3(b)] can be attributed to the spatial confinement of the sample, while the narrow distribution around $\vec{k}_y = 0$ [Fig. 3(c)] shows distinct maxima for the involved $\vec{k}$-vectors. These $\vec{k}$-vectors assemble the eigenmode along the long axis of the stripe at a given field and frequency configuration. Exemplary depictions of these measured eigenmodes are illustrated in subfigures (ii)–(v) in Figs. 3(b) and 3(c), respectively.

In the previous section, it was physically motivated to assume a sine-function as a representative for the investigated oscillations. One could argue that this motivation is weak as there may, for example, be multiple sine functions (i.e., Fourier components) involved in one oscillation or that the data does not represent a sine function at all but rather a simpler function. A simple test can now be performed by assuming different values for ω. Figure 4 shows the distribution of fit residuals under variation of ω, starting from $\omega = 0$ to $\omega = 2\omega_0$ in steps of $0.1\omega_0$. It appears that the residuals converge to a narrow Gaussian distribution at $\omega = \omega_0$, confirming the assumed frequency. Furthermore, the model itself can be motivated by trying simpler functions as models for the fit. For this purpose, we considered a Taylor expansion of the sine function. This yields a set of polynomials, starting from the 0th order and progressively approaching the sine function, where T_n denotes a Tailor series expansion to the nth order. The residuals as a function of the frequency for various polynomials in this series are depicted in Fig. 4. It is quickly

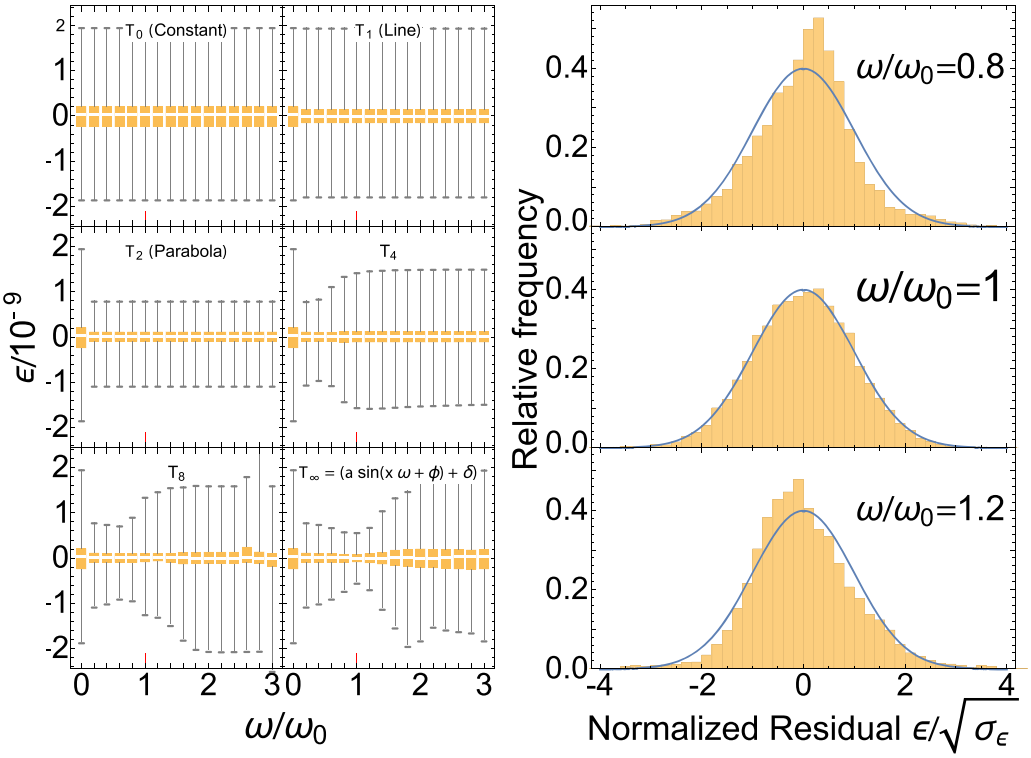

FIG. 4. Analysis of fit residuals. In this graphic, the concatenated residuals of the fits performed at each pixel in Fig. 2 are analyzed. To the left, the distribution of residuals ϵ is shown in the form of a box chart for various fit models as a function of frequency. The orange boxes indicate the margin within which half of the residuals are scattered, with a bright line near the center marking the median. The gray lines mark the positions of the minimal and maximal values of the residuals. To the right, the distribution of normalized residuals for the sin model [Eq. (5)] is depicted as a histogram. The normalization factor $\sqrt{\sigma_\epsilon}$ was calculated as the variance across the residuals. The orange bars mark the relative count rate for each value in the set of residuals. The blue curve is a Gaussian distribution of the form $\frac{1}{\sqrt{2\pi}} \exp\left(-\frac{x^2}{2}\right)$. A clear convergence to a narrow distribution is observed for the sine model at $\omega = \omega_0$. Simultaneously, the shape of the distribution of residuals near that value closely approximates a Gaussian distribution. This would be expected if the residuals were the result of random deviations or noise. Therefore, we can conclude that no additional signals are present in the observed data and that there is no polynomial function with three or fewer variables that has more explanatory power than the sine model [Eq. (5)].

noted that the convergence is best in only one case, namely, when using the sine-function with an assumed frequency of $\omega = \omega_0$. In this case, the residuals closely approximate a Gaussian distribution indicating that they are randomly distributed and not the result of a systematic deviation.

SUMMARY

We have demonstrated how magnonic contrast can be extracted from element-specific TR-STXM measurements with statistical rigor, even in the case of a few time steps. Not only can frequency and spatial phase-and-amplitude profiles be extracted, but a transposition to reciprocal space can be performed to identify the prevailing $\vec{k}$-vectors in a collective magnonic eigenstate. Our analysis can disentangle superimposed magnons depending on the excitation frequency, applied magnetic field, $\vec{k}$-vector, and phase. Furthermore, we have shown that our method is—beyond its physical motivation—statistically motivated. It carries statistical significance and allows quantitative deductions about the magnonic properties.

ACKNOWLEDGMENTS

This work was funded by the Deutsche Forschungsgemeinschaft (DFG, German Research Foundation) under Project Nos. OL513/1-1 and 321560838 and, in part, by the Deutsche Forschungsgemeinschaft (DFG, German Research Foundation) under Project No. 405553726 TRR 270. T.F. and H.O. acknowledge funding through Lawrence Berkeley National Laboratory LDRD Award: Development of a Continuous Photon Counting Scheme for Time Resolved Studies. T.F. acknowledges support from STROBE: A National Science Foundation Science & Technology Center, under Grant No. DMR-1548924. S.P and A.N. want to acknowledge funding by the Austrian Science Fund (FWF) under Project No. I-3050. B.Z. acknowledges helpful discussions with Michael Winklhofer. The authors acknowledge the use of the Stanford Synchrotron Radiation Lightsource, SLAC National Accelerator Laboratory, which is supported by the U.S. Department of Energy, Office of Science, Office of Basic Energy Sciences under Contract No. DE-AC02-76SF00515.

AUTHOR DECLARATIONS

Conflict of Interest

The authors have no conflicts to disclose.

Author Contributions

Benjamin Zingsem: Conceptualization (equal); Data curation (equal); Formal analysis (equal); Methodology (equal); Software (equal); Validation (equal); Visualization (equal); Writing – original draft (equal); Writing – review & editing (equal). **Thomas Feggeler**: Conceptualization (equal); Data curation (equal); Formal analysis (equal); Investigation (equal); Methodology (equal); Validation (equal); Visualization (equal); Writing – original draft (equal); Writing – review & editing (equal). **Ralf Meckenstock**: Conceptualization (equal); Funding acquisition (equal); Investigation (equal); Supervision (equal); Writing – review & editing (equal). **Detlef Spoddig**: Investigation (equal); Writing – review & editing (equal). **Taddäus Schaffers**: Writing – review & editing (equal). **Santa Pile**: Investigation (equal); Resources (equal); Writing – review & editing (equal). **Hendrik Ohldag**: Conceptualization (equal); Investigation (equal); Resources (equal); Writing – review & editing (equal). **Michael Farle**: Project administration (equal); Resources (equal); Supervision (equal); Writing – review & editing (equal). **Heiko Wende**: Project administration (equal); Resources (equal); Supervision (equal); Writing – review & editing (equal). **Andreas Ney**: Funding acquisition (equal); Project administration (equal); Supervision (equal); Writing – review & editing (equal). **Katharina Ollefs**: Conceptualization (equal); Funding acquisition (equal); Project administration (equal); Resources (equal); Supervision (equal); Writing – review & editing (equal).

DATA AVAILABILITY

The data that support the findings of this study are available within the article.[14]

REFERENCES

[1] M. Farle, "Ferromagnetic resonance of ultrathin metallic layers," Rep. Prog. Phys. **61**(7), 755 (1998).
[2] A. Khitun, M. Bao, and K. L. Wang, "Magnonic logic circuits," J. Phys. D: Appl. Phys. **43**(26), 264005 (2010).
[3] D. Grundler, "Reconfigurable magnonics heats up," Nat. Phys. **11**, 438 (2015).
[4] A. V. Chumak, V. I. Vasyuchka, A. A. Serga, and B. Hillebrands, "Magnon spintronics," Nat. Phys. **11**, 453 (2015).
[5] B. W. Zingsem, T. Feggeler, A. Terwey, S. Ghaisari, D. Spoddig, D. Faivre *et al.*, "Biologically encoded magnonics," Nat. Commun. **10**(1), 4345 (2019).
[6] A. Barman, G. Gubbiotti, S. Ladak, A. O. Adeyeye, M. Krawczyk, J. Gräfe *et al.*, "The 2021 magnonics roadmap," J. Phys.: Condens. Matter **33**, 413001 (2021).
[7] S. V. Vonsovskii, *The Phenomenon of Resonant Absorption of a High-Frequency Magnetic Field in Ferromagnetic Substances* (Pergamon Press, Oxford, London, Edinburgh, NY, Toronto, Paris, Frankfurt, 1966).
[8] S. O. Demokritov, B. Hillebrands, and A. N. Slavin, "Brillouin light scattering studies of confined spin waves: Linear and nonlinear confinement," Phys. Rep. **348**, 441–489 (2001).
[9] Y. Izyumov and R. P. Ozerov, *Magnetic Neutron Diffraction* (Plenum Press, New York, 1970).
[10] T. Chatterji, *Neutron Scattering from Magnetic Materials* (Elsevier, Amsterdam, Boston, Heidelberg, London, NY, Oxford, Paris, San Diego, San Francisco, Singapore, Sydney, Tokyo,2006).
[11] K. Koike and K. Hayakawa, "Scanning electron microscope observation of magnetic domains using spin-polarized secondary electrons," Jpn. J. Appl. Phys. **23**(Part 2, No. 3), L187–L188 (1984).
[12] T. Balashov, A. F. Takács, W. Wulfhekel, and J. Kirschner, "Magnon excitation with spin-polarized scanning tunneling microscopy," Phys. Rev. Lett. **97**, 187201 (2006).
[13] S. Bonetti, R. Kukreja, Z. Chen, D. Spoddig, K. Ollefs, C. Schöppner *et al.*, "Microwave soft x-ray microscopy for nanoscale magnetization dynamics in the 5-10 GHz frequency range," Rev. Sci. Instrum. **86**(9), 093703 (2015).
[14] S. Pile, T. Feggeler, T. Schaffers, R. Meckenstock, M. Buchner, D. Spoddig *et al.*, "Non-standing spin-waves in confined micrometer-sized ferromagnetic structures under uniform excitation," Appl. Phys. Lett. **116**(7), 072401 (2020).
[15] T. Feggeler, R. Meckenstock, D. Spoddig, B. W. Zingsem, H. Ohldag, H. Wende *et al.*, "Spatially resolved GHz magnetization dynamics of a magnetite nanoparticle chain inside a magnetotactic bacterium," Phys. Rev. Res. **3**(3), 033036 (2021).
[16] L. Körber, M. Zimmermann, S. Wintz, S. Finizio, M. Kronseder, D. Bougeard *et al.*, "Symmetry and curvature effects on spin waves in vortex-state hexagonal nanotubes," Phys. Rev. B **104**, 184429 (2021).

[17]E. Albisetti, D. Petti, G. Sala, R. Silvani, S. Tacchi, S. Finizio *et al.*, "Nanoscale spin-wave circuits based on engineered reconfigurable spin-textures," Commun. Phys. **1**(1), 56 (2018).
[18]E. Albisetti, S. Tacchi, R. Silvani, G. Scaramuzzi, S. Finizio, S. Wintz *et al.*, "Optically inspired nanomagnonics with nonreciprocal spin waves in synthetic antiferromagnets," Adv. Mater. **32**(9), 1906439 (2020).
[19]J. Stöhr and H. C. Siegmann, *Magnetism* (Solid-State Sciences Springer, Berlin, Heidelberg, 2006), **5**.
[20]F. Groß, N. Träger, J. Förster, M. Weigand, G. Schütz, and J. Gräfe, "Nanoscale detection of spin wave deflection angles in permalloy," Appl. Phys. Lett. **114**(1), 012406 (2019).
[21]W. Chao, P. Fischer, T. Tyliszczak, S. Rekawa, E. Anderson, and P. Naulleau, "Real space soft x-ray imaging at 10 nm spatial resolution," Opt. Express **20**(9), 9777–9783 (2012).
[22]R. Narkowicz, D. Suter, and R. Stonies, "Planar microresonators for EPR experiments," J. Magn. Reson. **175**(2), 275–284 (2005).